HAL
open science

Active hydrothermal vents in the Woodlark Basin may act as dispersing centres for hydrothermal fauna

Cédric Boulart, Olivier Rouxel, Carla Scalabrin, Pierre Le Meur, Ewan Pelleter, Camille Poitrimol, Eric Thiébaut, Marjolaine Matabos, Jade Castel, Adrien Tran Lu y, et al.

To cite this version:

Cédric Boulart, Olivier Rouxel, Carla Scalabrin, Pierre Le Meur, Ewan Pelleter, et al.. Active hydrothermal vents in the Woodlark Basin may act as dispersing centres for hydrothermal fauna. Communications Earth & Environment, 2022, 3, pp.64. 10.1038/s43247-022-00387-9 . hal-03611693

HAL Id: hal-03611693

https://hal.science/hal-03611693

Submitted on 17 Mar 2022

HAL is a multi-disciplinary open access archive for the deposit and dissemination of scientific research documents, whether they are published or not. The documents may come from teaching and research institutions in France or abroad, or from public or private research centers.

L'archive ouverte pluridisciplinaire **HAL**, est destinée au dépôt et à la diffusion de documents scientifiques de niveau recherche, publiés ou non, émanant des établissements d'enseignement et de recherche français ou étrangers, des laboratoires publics ou privés.

communications
earth & environment

ARTICLE

https://doi.org/10.1038/s43247-022-00387-9 OPEN

Active hydrothermal vents in the Woodlark Basin may act as dispersing centres for hydrothermal fauna

Cédric Boulart[1✉], Olivier Rouxel[2], Carla Scalabrin[2], Pierre Le Meur[3], Ewan Pelleter[2], Camille Poitrimol[1,4], Eric Thiébaut[1], Marjolaine Matabos[4], Jade Castel[1], Adrien Tran Lu Y[5,6], Loic N. Michel[4], Cécile Cathalot[2], Sandrine Chéron[2], Audrey Boissier[2], Yoan Germain[2], Vivien Guyader[2], Sophie Arnaud-Haond[7], François Bonhomme[5], Thomas Broquet[1], Valérie Cueff-Gauchard[8], Victor Le Layec[1,6], Stéphane L'Haridon[8], Jean Mary[1], Anne-Sophie Le Port[1], Aurélie Tasiemski[9], Darren C. Kuama[10], Stéphane Hourdez[6] & Didier Jollivet[1]

Here we report the discovery of a high-temperature hydrothermal vent field on the Woodlark Ridge, using ship-borne multibeam echosounding and Remotely Operated Vehicle (ROV) exploration. La Scala Vent Field comprises two main active areas and several inactive zones dominated by variably altered basaltic rocks, indicating that an active and stable hydrothermal circulation has been maintained over a long period of time. The Pandora Site, at a depth of 3380 m, is mainly composed of diffuse vents. The Corto site, at a depth of 3360 m, is characterized by vigorous black smokers (temperature above 360 °C). The striking features of this new vent field are the profusion of stalked barnacles *Vulcanolepas* sp. nov., the absence of mussels and the scarcity of the gastropod symbiotic fauna. We suggest that La Scala Vent Field may act as a dispersing centre for hydrothermal fauna towards the nearby North Fiji, Lau and Manus basins.

[1] UMR 7144 AD2M CNRS-Sorbonne Université, Station Biologique de Roscoff, Place Georges Tessier, 29680 Roscoff, France. [2] IFREMER REM-GM, Technopôle Brest Plouzané, 29280 Plouzané, France. [3] GENAVIR, Technopôle Brest Plouzané, 29280 Plouzané, France. [4] IFREMER REM-EEP, Technopôle Brest Plouzané, 29280 Plouzané, France. [5] ISEM CNRS UMR 5554, Université de Montpellier 2, 34095 Montpellier Cedex 5, France. [6] UMR 8222 LECOB CNRS-Sorbonne Université, Observatoire Océanologique de Banyuls, Avenue du Fontaulé, 66650 Banyuls-sur-mer, France. [7] IFREMER UMR 248 MARBEC, Avenue Jean Monnet CS 30171, 34203 Sète, France. [8] Univ. Brest, Ifremer, CNRS, Laboratoire de Microbiologie des Environnements Extrêmes UMR6197, F-29280 Plouzané, France. [9] Univ. Lille, CNRS, Inserm, CHU Lille, Institut Pasteur de Lille, U1019-UMR9017-CIIL-Centre d'Infection et d'Immunité de Lille, Lille, France. [10] PNG Science and Technology Secretariat, University of Papua New Guinea, Port Moresby, Papua New Guinea. ✉email: cedric.boulart@sb-roscoff.fr

Hydrothermal venting on the deep seafloor is the manifestation of heat and matter transfer from the lithosphere to the oceans, which modify their geochemical composition[1]. Upon mixing with the surrounding, cold, deep-sea water, a precipitation occurs and forms sulfide deposits on the seafloor. These hot and acidic fluids sustain diverse chemical-based ecosystems where large specialized bacterial and animal communities can thrive under extreme conditions of temperature, pressure, and pH[2]. Since the observation of the first active high-temperature vents more than 40 years ago[3], the exploration of the deep ocean has revealed the existence of hydrothermal circulation in a wide range of geological settings from fast-spreading ridges[4] to ultra-slow ones[5] as well as in intraplate hotspots[6], subduction zones[7], and back-arc basins[8].

Economic and societal interest in deep-sea hydrothermal vents has increased in the recent years because of the formation of massive polymetallic sulfide deposits[9] that are now targeted for deep-sea mining[10], which may impact the deep ocean environment. The Woodlark Basin, located South of the Solomon Islands arc region in the Western Pacific Ocean, is a rather young (~5–7 Mya) oceanic basin that is subducting beneath the New Britain-San Cristobal Trench (Fig. 1). This is in fact one of the only places on Earth where an active spreading centre expands into both continental crust to the West, and is bound by a subduction zone to the East[11,12], therefore offering a wide range of geotectonic constraints for the development of seamounts and the possibility of forming high and low temperature hydrothermal venting along the axis. This may then provide a great diversity of niches for hydrothermal fauna and microbial colonization, and the potential settlement of associated fauna, provided that venting sites remain active over a long period of time.

The Woodlark Basin is characterized by an E–W active spreading axis that Goodliffe et al.[13] divided into five segments, numbered 1 through 5 from West to East (Fig. 1). The bathymetry shows major differences between the Eastern and Western parts, separated by the Moresby Transform Fault (TF), with a significantly shallower seafloor to the West, and a well-developed axial graben to the East[14]. Spreading rates vary from 38 mm yr^{-1} in the West, to 67 mm yr^{-1} on the Eastern part[15]. Hydrothermal activities are known to occur on only three segments of the ridge, which include confirmed volcanic activity on Segment 1 (Franklin Seamount[11]), and inferred hydrothermal venting thought to be due to punctual eruptive phases on Segment 3 and Segment 5[12]. Although recent exploration found consistent turbidity and redox

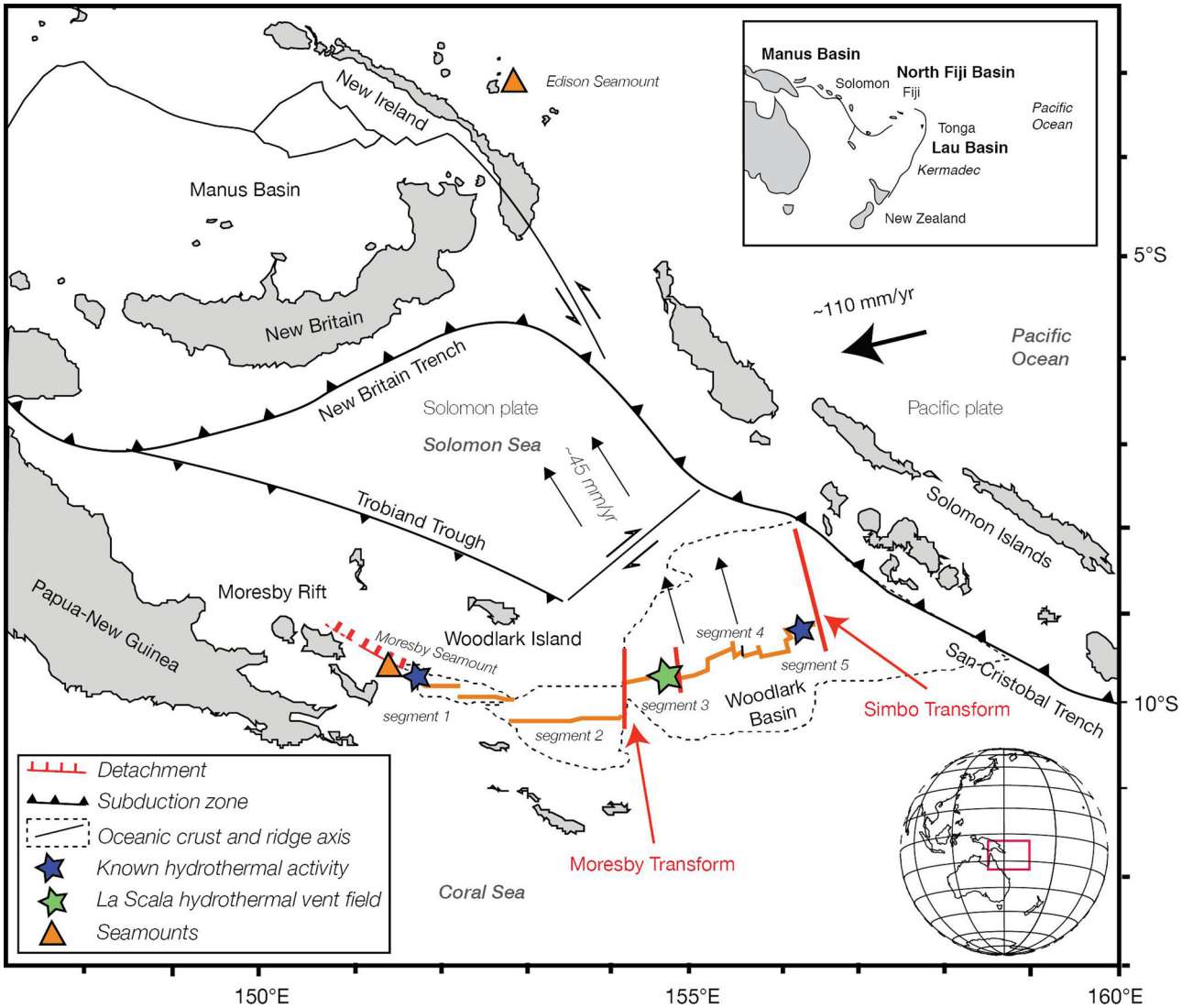

Fig. 1 Regional map of the Woodlark Basin. The main tectonic settings are highlighted as well as the location of the newly discovered 'La Scala' hydrothermal vent field (green star), modified from Laurila et al. (2012)[12]. Black arrows indicate the directions of plate motion relative to a fixed Australian plate.

potential anomalies at 2900 m below sea level (mbsl) over the eastern edge of Segment 3, Laurila et al.[12] concluded that "the complexity of the tectonics, i.e., frequent ridge jumps and re-orientation of the spreading axis, prevents high-temperature venting in one stable location and, hence the formation of sea-floor massive sulfide deposits", suggesting that stable deep-sea vent communities may not be able to establish there.

Although not reported, the presence of perennial hydrothermal vent fields in the Woodlark Basin could constitute a stepping stone for hydrothermal fauna, at the intersection between the Manus Basin, the Edison Seamount, and the North Fiji and Lau basins, because of its possible link to the Northern expansion of the North Fiji basin which started about 10–11 Mya[16]. This spreading centre, now subducted, was presumed to bridge the older -and fossil- Solomon and South Fiji ridges that shaped the region before the collision of the Melanesian arc and the Ontong Java plateau about 18 Mya[17]. This collision coincides with the oldest dates of speciation events in the complex of gastropod species *Alviniconcha* which initiated 20 Mya[18]. The Woodlark Basin is older than the currently active spreading centres of the adjacent Lau (1–2 Ma) and North Fiji (3–4 Ma) basins, and therefore, may act as a biodiversity dispersion centre for the modern hydrothermal vent fauna at a crossroad between the Manus, North Fiji, and Lau basins.

During the CHUBACARC 2019 cruise (https://doi.org/10.17600/18001111), we carried out an extensive water-column survey of the eastern edge of Segment 3, using a strategy based on ship-borne acoustic survey followed by CTD-casts, to detect both thermal and chemical anomalies near the location where Laurila et al.[12] previously reported activity. Based on these observations, we then conducted a seafloor survey using the ROV Victor 6000 that led to the discovery of several high-temperature hydrothermal black smokers. Here, we report on the acoustic and chemical characterization of the hydrothermal plumes, the composition of endmember fluids, the geological setting of the vent fields, and the composition of the fauna associated with the newly discovered vent field we named 'La Scala'.

Results and discussion

Hydrothermal plume exploration over the Eastern Woodlark Ridge. As part of the high-resolution mapping—using the ship-borne multibeam echosounder (EM122 12 kHz)—carried out over Segment 3 (Fig. 2a), the water column imaging survey revealed the presence of echoes rooted to the seafloor in the vicinity of the 'TVG-150' marker[15]. These echoes, rising 200–300 m above the seafloor (Fig. 2b, Supplementary Fig. 1), remained visible at the same location at each passage of the ship over the area and showed the same features as the plumes previously observed in the Guaymas Basin[19]. During the CHUBACARC cruise, similar signals were also observed at shallower sites known to host active vents in the Manus Basin. These echoes were therefore attributed to the presence of hydrothermal plumes. It is commonly believed that deep hydrothermal plumes cannot be detected by water column acoustic imaging because of the absence of strong scatterers such as gas bubbles or droplets[20]. However, Ondréas et al.[19] showed that hydrothermal plumes down to 2000 mbsl could be identified using ship-borne multibeam echosounding and differentiated from gas and liquid emissions. In the case of La Scala plumes, the backscattering mechanism may result from a combination of turbulence-induced temperature fluctuations within the first tens of metres of the vents and the presence of fine particles over the entire field at 100–500 m above the seafloor, which was later confirmed by the CTD surveys over the area (very strong turbidity signal and temperature anomalies >0.2 °C in the buoyant plume) and the subsequent ROV dives. By modelling the acoustic characteristics of the hydrothermal plumes, Xu et al.[21] showed that particles had a predominant role in the acoustic backscatter with the height above the vents. It is worth noting that the success of this technique of detection strongly depends on the acoustic impedance difference between the hydrothermal fluid and the surrounding water, on the acoustic frequency, and on the sea state.

The subsequent CTD/tow-yo survey (Fig. 2c) first in the N–S direction and, then followed by a NE–SW transect crossing above the fluid echo showed turbidity (or nephelometry) anomalies at 2800 and 3300 mbsl i.e., at an altitude of 300–500 m above the seafloor (Fig. 3a, b), associated to manganese (Mn) anomalies (up to ~108 nM, Supplementary Data 1) and redox potential (Eh) signals. The strongest anomalies appeared to be consistent with the location of the echoes, confirming the presence of a buoyant plume.

The second phase of the water column survey consisted of two vertical CTD casts (CTD-06 and CTD-07) above the strongest acoustic and chemical anomalies spotted during the MBES and the tow-yo survey. The data showed unambiguous anomalies of Eh, pH, potential temperature, density, and turbidity (Fig. 3c, d), which confirmed the presence of both buoyant and non-buoyant plumes. During CTD-06, we encountered a first turbidity anomaly (0.08 NTU) associated to an Eh signal at 2850 mbsl corresponding to a dispersing buoyant plume 500 m above seafloor. Below, a second, weaker turbidity anomaly (0.03 NTU) was found but not associated to any other chemical signal. Finally, very strong turbidity signals (up to 0.5 NTU), as well as temperature anomalies (~0.1–0.3 °C), were observed close to the seafloor (180 and 100 m above the seafloor) indicative of the presence of at least two hydrothermal plumes (Supplementary Fig. 2). The CTD-07 cast, conducted a few hours later and 60 m away from the CTD-06 location, showed a typical non-buoyant plume structure for turbidity and temperature (anomalies > 0.2 °C), as well Mn varying from 34 to 265 nM. The CTD-07 vertical profile clearly indicated the presence of several black smoker-type sources spread out on the flank of the ridge, from 3300 to 3500 mbsl. These vents seem to generate a regional neutrally-buoyant plume dispersing northeastward at 2800–2850 mbsl.

Based on these exploratory results, an ROV dive close to the bottom led to the discovery of many active hydrothermal chimneys (i.e., black smoker types) and complex spires located between 3300 and 3400 mbsl, as well as a large diffuse venting area colonized by extensive communities of stalked barnacles (Fig. 4). The new vent field, discovered at coordinates 9°47S/155°03E was named 'La Scala', in recognition of the acoustic eyes of its discoverer.

Three additional CTD casts (CTD-08, 09, and 10, Fig. 2c) were carried out to estimate the dispersion of the plumes. While the CTD-08 profile showed some clear evidence of hydrothermal plumes dispersing at 2800–2900 mbsl, no anomalies were observed on the CTD-09 and CTD-10 profiles, located at 2.4 and 5.7 km, south and southwest of CTD-07, respectively (Supplementary Data 1). This may indicate a strong control of the dispersion of the plumes by the topography.

Field observations of the La Scala Vent Field

La Scala Vent Field (LSVF) is located at a distance of 1.2 km North of the neovolcanic axis on the northern part of an old split axial volcanic ridge. The LSVF lies on a NE-trending talus slope and is composed of two main active areas and several zones with inactive chimneys (Fig. 2b). The first active site, named 'Pandora', is located Southeast of the field at 3380 mbsl and extends some 30 m by 10 m. It is characterized by predominantly diffusive vents, a few black smokers (Fig. 4a, b) and

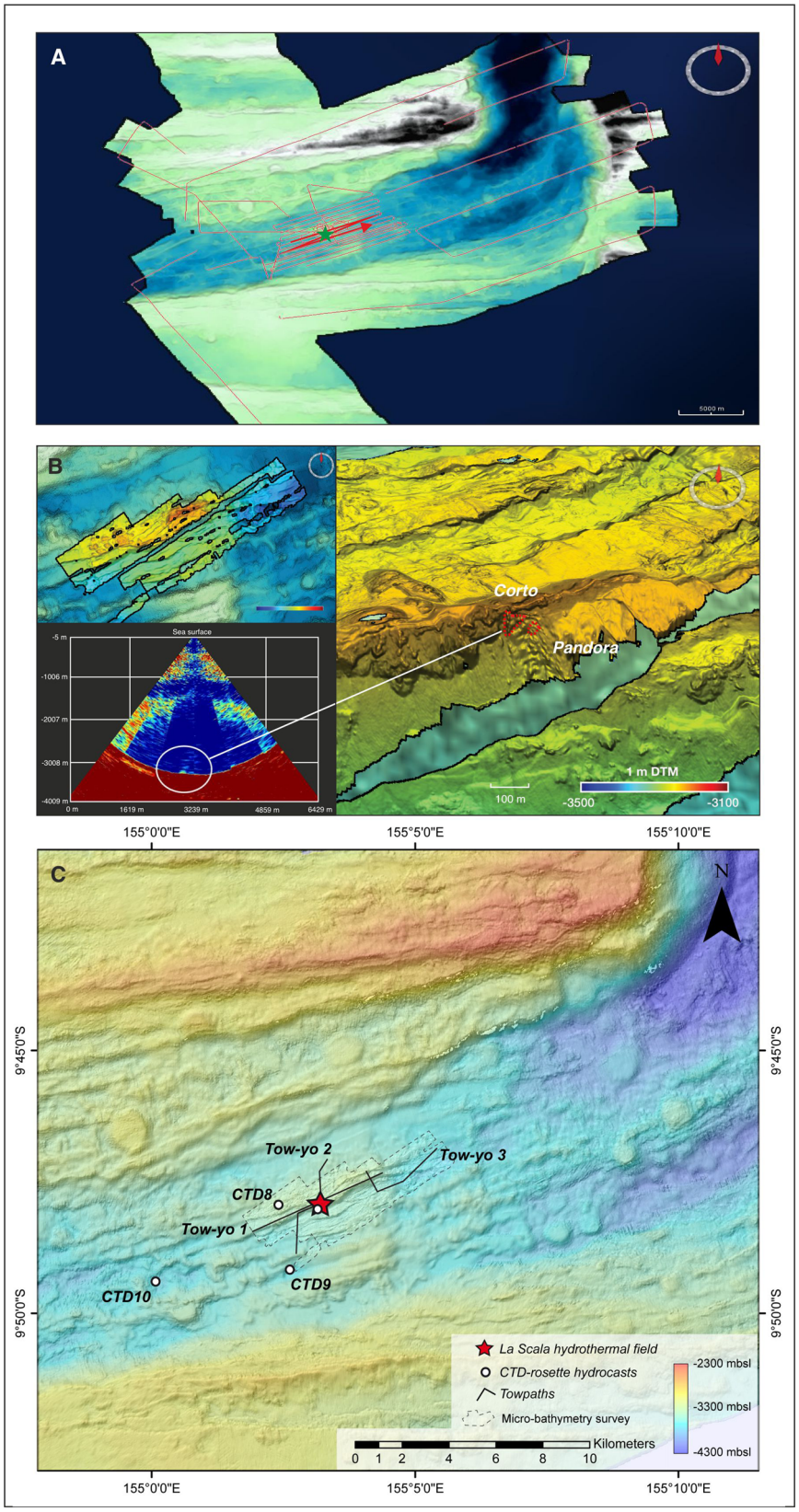

extinct chimneys N20 aligned and colonized by an extensive coverage of stalked barnacles and patches of gastropods. The second active site of the field, named 'Corto', lies along a steeper slope at 3360 mbsl, only 15–20 m Northwest of the first site. It comprises a 50 m by 15 m sulfide zone where several 7–10 m tall, vigorous, high-temperature black smokers (Temperature ranging from 364 to 366 °C, Table 1, Fig. 4c, d) were observed at the Southern edge.

Active hydrothermal chimneys are located on steep talus composed of hydrothermally encrusted basaltic rubble, chimneys fragments, and white blocks of hydrothermally altered volcanic rocks. Near the summit, just above the Corto site, a 30 m tall cliff

Fig. 2 La Scala Vent Field bathymetry. A Chubacarc cruise bathymetry image (20 m grid DTM (Digital Terrain Model), ship-borne MBES) corresponding to the water column acoustic surveys of the Woodlark Ridge (segment 3b). The green star locates the 'La Scala' hydrothermal field. **B** Northward 3D view of the high-resolution bathymetry image (1 m grid DTM, ROV VICTOR MBES) overlaid on the greyed 20 m grid DTM corresponding to the northern part of the old split axial volcanic ridge where LSVF is located. La Scala Vent Field including Pandora and Corto sites is delimited by the red dashed line, on the southern flank of the ridge together with the post-processed echogram of the second profile showing the echo attributed to LSVF. **C** Bathymetry of the segment 3 of the Woodlark Ridge from shipboard multibeam survey showing the location of LSVF as well as the towpaths and the CTD-hydrocasts. Note that CTD06 and CTD07 are located right above LSVF. TVG-150 spot from Laurila et al. (2012)[12] is not showed for clarity as it is 140 m away from LSVF.

is composed of pillow lavas topped by massive lava flows (Fig. 4e). On this same cliff, fifty metres Southwest of the second hydrothermal site, pervasive alteration zones and possibly oxidized massive sulfides exposed after a tectonic event (Fig. 4f) have been observed, indicating past hydrothermal activity in the area. Even though high-temperature chimneys could have formed during previous hydrothermal episodes, most ancient sulfide structures were probably destroyed during a collapse. Thus, at least two hydrothermal events occurred at LSVF. Based on the spreading rate (~ 50 mm yr^{-1}) and the distance from the neo-volcanic axis (~1.2 km), the maximum age of the first event of hydrothermal activity at LSVF can be estimated to be 24,000 years ago. This calculation, along with the presence of numerous inactive chimneys and altered lava, clearly indicates that an active and stable hydrothermal circulation has been maintained over a certain period of time and may not be the result of a recent and episodic volcanic eruption as previously suggested[12].

Petrological and geochemical characteristics

Basement rocks recovered at LSVF are composed of rounded to sub-angular clasts of non-vesicular aphyric to plagioclase-pyroxene-phyric basalt (cm-size pebbles), cemented by a silica-rich matrix (quartz and cristobalite) and often coated by mm-thick iron oxyhydroxide crust. Pyrite and minor sphalerite are also identified by X-ray diffraction (XRD) confirming the importance of hydrothermal fluid circulation in basement rock alteration at LSVF. East of the vent field along the summit of the ridge crest, recovered basement rocks consisted of essentially aphyric and non-vesicular pillow lava with glassy chilled margin. Incipient to no alteration was identified. The volcanic crest is covered by thin sediment dusting composed of nanofossil-bearing clay.

Geochemical analyses of volcanic rocks show silica contents ranging from 48.4 to 48.7 wt% and low alkali contents ($Na_2O + K_2O$) from 2.7 to 2.9 wt% (Supplementary Table 1). Thus, all samples from the LSVF area are tholeiitic basalt similar to mid-ocean ridge basalt (MORB) composition (Supplementary Fig. 3). Glassy pillow margins contain 9.1–9.5 wt% MgO suggestive of rather primitive melt. To our knowledge, these are the first report of basaltic rock composition along Segment 3 of the Woodlark Basin in agreement with the previous studies along Eastern Segment 4[22,23] and consistent with MORB composition with major element variations resulting from fractional crystallization.

Sulfide deposits and hydrothermal fluids

Three different types of mineralization (Fig. 4 and Supplementary Data 2) were observed and sampled during the subsequent ROV dives: (1) active high-temperature sulfide/sulfate chimneys without significant presence of sessile animals; (2) inactive black smoker chimneys; (3) massive sulfide recovered at the base of either active or inactive complex spire densely colonized by vent organisms. Mineralogical and petrological descriptions show that anhydrite is the dominant mineral in the top section of active black smoker chimney, followed by chalcopyrite, sphalerite, and pyrite towards the inner and lower section of the chimney. Multiple vigorously venting internal conduits are lined with fine grained euhedral chalcopyrite while chimney walls are composed of mixed mineral assemblages of chalcopyrite, sphalerite, and pyrite. Inactive chimneys and massive sulfides have essentially similar characteristics to active chimney except that anhydrite is absent due to retrograde dissolution and chimney wall are consolidated by more massive pyrite/marcasite assemblages, and thinly encrusted by Fe oxyhydroxide crust.

Sulfide deposits show a wide range of copper (Cu) and zinc (Zn) concentrations reflecting the abundances of chalcopyrite versus sphalerite, while calcium (Ca), strontium (Sr), and silica (Si) reflect the abundance of anhydrite and silica respectively (Suppl. Data 3). As previously recognized[24], trace elements such as cadmium (Cd) and lead (Pb) are associated with lower-temperature sphalerite-rich mineral assemblages. Average compositions are relatively similar between sulfide deposits, except for the Carioca black smoker characterized by lower Cu and higher cobalt (Co) concentration, up to 0.6 wt% in pyrite-rich samples. High Co contents in basalt-hosted sulfide chimneys have been previously inferred as reflecting a higher magmatic contribution to the hydrothermal fluid[24]. By comparison with average compositions of sulfide mineralization in other tectonic environments in the modern seafloor, LSVF lacks any of the geochemical features of back-arc settings (e.g., gold and Pb enrichment) and is seemingly identical to other basalt-hosted hydrothermal fields along mid-oceanic ridges.

Sulfur isotope analysis was performed on the mineral fractions of pyrite and chalcopyrite of four samples, yielding a range of $\delta^{34}S$ values between 1.96‰ and 4.20‰, with an average of 3.03 ‰ (Supplementary Data 3). Slightly higher $\delta^{34}S$ values in the Carioca black smoker indicate a seawater contribution to the hydrothermal fluid in the upflow zone. Such $\delta^{34}S$ values are typical of sulfide mineralization from mid-oceanic ridge settings (Supplementary Fig. 4) and suggest no contribution of magmatic SO_2 ($\delta^{34}S < 0$‰) as encountered in back-arc basin hydrothermal systems (e.g., Lau Basin and Manus Basin). Altogether, these results are consistent with the basaltic rock composition and indicate that the magmatic activity on the ridge segment is not directly related to subduction but rather to accretion.

Hydrothermal vent fluids were recovered from three black smoker chimneys from LSFV, all showing remarkably homogeneous venting temperature of ~365 °C (Table 1 and Supplementary Table 2). All recovered vent fluids have non-zero magnesium (Mg) concentrations due to significant seawater entrainment during sampling. Endmember composition of vent fluids are conventionally assumed to be devoid of Mg, because of the quantitative removal of Mg from seawater during hydrothermal interactions with basalt[25,26]. Calculated end-member hydrothermal fluid compositions are reported in Table 1 for all measured elements.

Homogeneous end-member compositions suggest that LSVF is fed by a deep-seated hydrothermal fluid source undergoing minor subsurface fluid mixing. The lowest pH value (3.31) was recorded in Carioca vent fluids consistent with the lowest Mg concentration of 1.6 mM, which suggests minor seawater contribution during sampling. Hence, the end-member pH value is considered to be close to 3.3 for all vents. All end-member vent fluids have

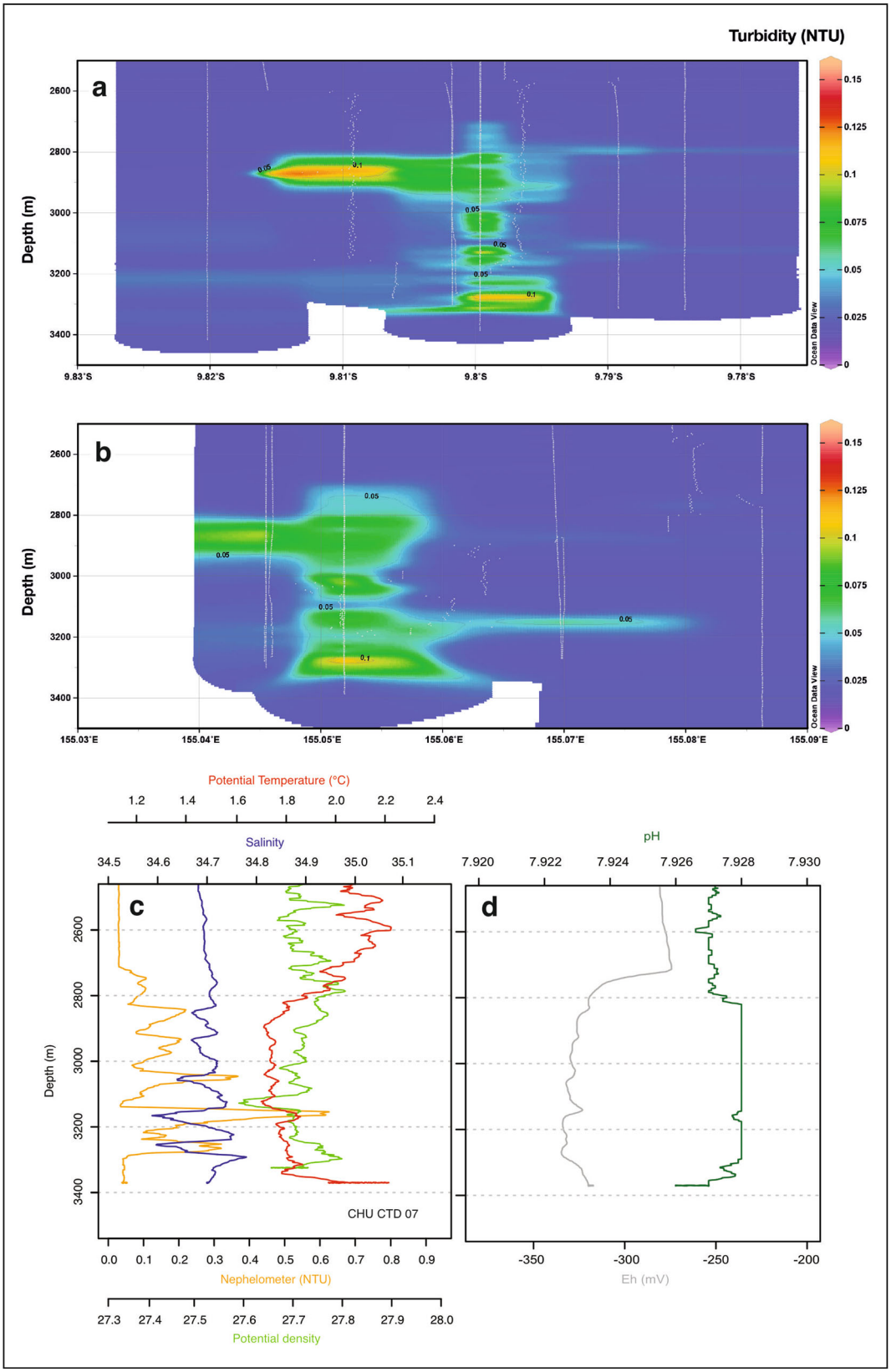

Fig. 3 Physico-chemical characteristics of hydrothermal plumes above La Scala Vent Field. N-S (**a**) and NE-SW (**b**) sections of turbidity anomalies above Segment 3. The section compiles data from tow-yo surveys (CTD-01 to CTD-03) and vertical casts (CTD-06 and CTD-07) (grey lines). **c**, **d** Nephelometry (yellow), density (light green), salinity (blue), temperature (red), Eh (grey), and pH (dark green) vertical profiles in the non-buoyant plume of 'La Scala' vent site (CTD-07).

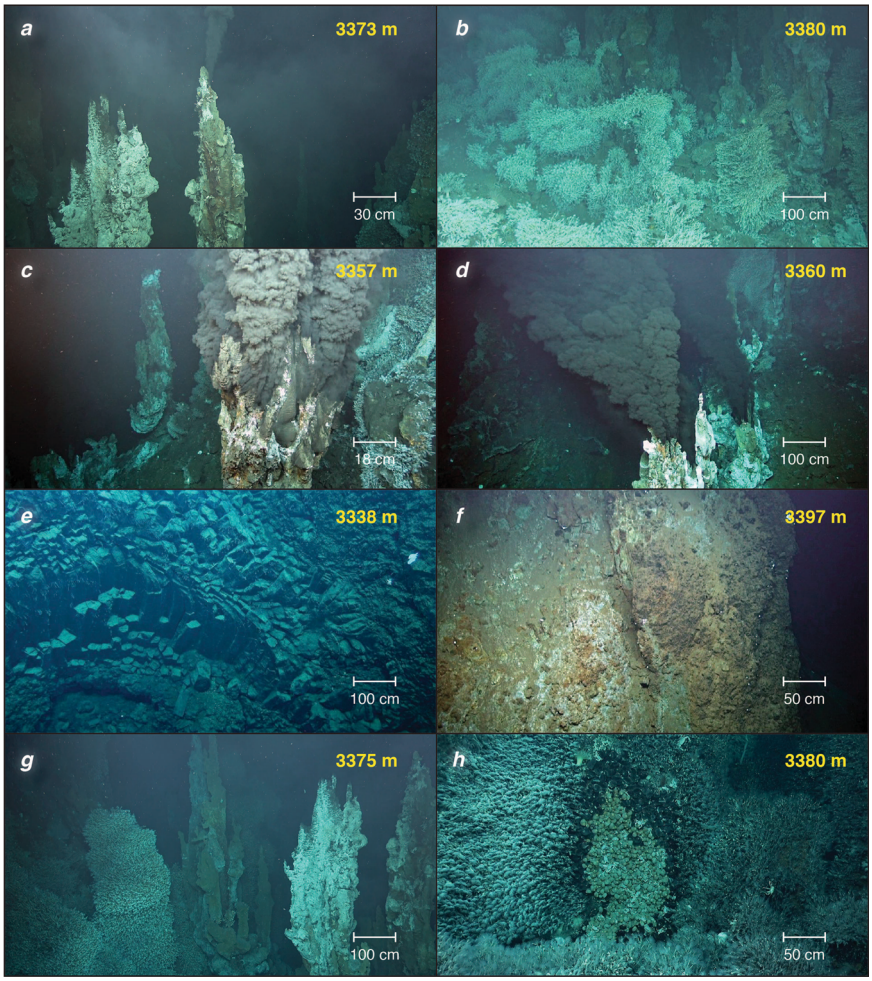

Fig. 4 La Scala Vent Field. a, **b** Chimney cluster ('Pandora Site'), SE of the vent field at 3380 m depth characterized by a few black smokers and predominant weakly diffusive vents. This site is surrounded by cirripeds to the West, North and East. **c**, **d** Second site ('Corto Site') located on the flank of a cliff controlled by a N55-60 fault. The South area at 3360 m depth is the most active of the hydrothermal field. **e** Massive prismatic lava. **f** Highly altered basalts due to past high temperature hydrothermal circulation. **g** Large colonies of *Vulcanolepas* sp. colonizing inactive chimneys. **h** A patch of *Alviniconcha* endosymbiotic gastropods surrounded by *Ifremeria nautilei* and *Vulcanolepas* sp.

chlorinities higher than seawater suggesting they have undergone sub-critical phase separation. Alkali concentrations (K≈25.4 mM; Rb ≈ 15.6 μM) are similar to most basaltic-hosted vent sites consistent with LSVF geological setting. Silica (Si), iron (Fe) and Mn concentrations are ≈20 mM, ≈1.7 mM, and ≈1.0 mM, respectively. Fe/Mn ratio of 1.7 is however lower than values expected from the vent temperature[27], suggesting possible subsurface sulfide precipitation. Endmember Cu and H_2S concentration of 21 μM and 4.1 mM respectively, are also lower than typical high temperature (i.e., >350 °C) vent fluids, lending further support to this hypothesis.

Hydrothermal vent fauna

LSVF is characterized by several very active black smoker chimneys whose surface is occupied by a sparse population of *Rimicaris* shrimp and very large beds of a new species of stalked barnacles, *Vulcanolepas* sp. nov., that colonizes mildly active diffuse venting areas and old inactive chimneys or sulfide mounds (Fig. 4g). The dominant engineer species and their associated fauna were comparable to other Southwest Pacific vent communities but differed in relative abundance[28–30]. Stalked barnacles covered vast areas (c.a. >300 m^2) on the seafloor while large symbiotic gastropods were rare and restricted to patches smaller than in other Western Pacific back-arc basins. Patches of small-sized gastropods *Ifremeria nautilei* and *Alviniconcha* spp. were observed in the most active diffuse areas with temperatures varying from 2.4 to 7.3 °C (average of 4.6 ± 1.3 °C) and 2.5–20.3 °C (average 8.5 ± 4.4 °C), respectively (Fig. 4h). Cirripeds *Eochinelasmus ohtai* and *Imbricaverruca* sp. were found next to *Ifremeria nautilei* and *Alviniconcha* spp. communities (Fig. 5). Aggregations of alvinocaridid shrimp *Rimicaris variabilis*, *Branchinotogluma segonzaci* polynoids, and *Shinkailepas tufari* phenacolepadid gastropods were also observed on active chimneys (Fig. 5f). Extensive bacterial mats were also noticed at the periphery of the vents, as well as bamboo corals (Isididae), squat lobsters (Munidopsidae), brisingid starfish, crinoids, and sea anemones (Supplementary Fig. 5). Morphological identification of the benthic fauna collected and observed from videos was compiled as a list of at least 45 taxa, including 23 families and 23 genera (Supplementary Data 4). The macrofauna associated with *Vulcanolepas* sp. nov. was mainly composed of the barnacle *Imbricaverruca* sp., members of the polychaete families Ampharetidae (*Amphisamytha* cf. *vanuatuensis*), Maldanidae (*Nicomache* spp.), and Spionidae, and the provannid gastropod *Provanna* sp. (Supplementary Data 5). Many copepods and nematodes were also part of this community. Holothurians *Chiridota* sp., anemones (Actiniaria), squat lobsters, *Austinograea*

Table 1 Temperature, pH, and chemical composition of La Scala fluid endmembers.

	Temp (°C)	pH (21 °C)	H_2S mM	Mg mM	Cl mM	SO_4 mM	Na mM	S mM	K mM	Ca mM	Sr µM	Li µM	B µM	Rb µM	Cd µM	Ba µM	Si µM	Mn µM	Fe µM	Cu µM	Zn µM
Bottom SW		7.5	0.00	55.75	546	28.2	474	29.8	9.1	10.6	99	27	435	1.5	<0.1	0.08	122	<0.1	<1	<0.1	<0.1
Black smoker 6	364	<4.31	>2.2	0	633.2	2.0	561	2.7	25.3	31.7	115	1163	763	15.6	0.2	9.4	20074	1019	1602	39.9	108.1
Black smoker 5	366	3.3	4.0	0	634.9	1.4	543	2.1	25.4	31.0	115	1208	749	15.6	0.1	17.1	19795	1019	1848	10.8	50.6
Black smoker 8	365	3.3	4.1	0	647.9	1.5	548	5.4	25.6	31.5	115	1198	757	15.6	0.1	14.6	20122	1028	1707	12.6	39.8

crabs and *Phymorhynchus* sp. gastropods were also found among and next to *Vulcanolepas* sp. nov. thickets. A sample collected in an *Ifremeria nautilei* patch showed that the associated macrofauna was dominated by an undescribed peltospirid limpet and polynoid scaleworms, and formed the most diverse assemblage in term of species richness. *Amphysamytha* cf. *vanuatensis* and alvinellid worms (genus *Paralvinella*) were also found in *Ifremeria nautilei* and *Alviniconcha* spp. communities. Copepods, bythograeid crabs (*Austinograea* sp., which is likely to represent a new species), *Rimicaris variabilis* shrimp and polychaetes were the dominant taxa found in *Alviniconcha* spp. patches.

Most of the fauna had $\delta^{34}S < 10‰$ (Fig. 6), suggesting they primarily depend (either directly or indirectly) on chemosynthetic vent production and sulfide oxidation for their nutrition[31]. This was notably the case of organisms considered as peripheral fauna, or not strictly found at vents, such as *Vulcanolepas* sp. nov., anemones, or *Phymorhynchus* sp.. Brisingidae starfish, holothurians *Chiridota* sp., and carnivorous sponges had $\delta^{34}S$ between 10 and 15‰, suggesting a mixed diet, depending on both chemosynthesis- and photosynthesis-derived organic matter[31]. Only the Isididae bamboo corals had a $\delta^{34}S$ greater than 15‰, suggesting they primarily feed on exported photosynthetic production[31]. Overall, the dependence of organisms on vent endogenous production seemed significant, and spanned all sampled taxonomic and functional groups. Similar observations have been made in active[32] and inactive[33] hydrothermal vents from the Manus basin. In contrast, the dependence of hydrothermal fauna on exported photosynthetic matter is higher at shallower vents of the Southern Tonga arc[34]. The increased importance of endogenous production for deeper sites matches patterns observed in other chemosynthesis-based habitats[35,36].

While $\delta^{34}S$ values ruled out major photosynthetic contributions, the wide ranges of $\delta^{13}C$ and $\delta^{15}N$ measured in Woodlark fauna suggest that animal communities show considerable trophic diversity, and depend on several production mechanisms (Fig. 6). Some species had very negative $\delta^{13}C$ (e.g., *Alviniconcha kojimai*, *Ifremeria nautilei* or *Provanna* sp.), suggesting they mostly depend on sulfide oxidizers using the Calvin–Benson–Bassham (CBB) cycle for their nutrition[37]. Conversely, some species, such as *Alviniconcha boucheti* or *Branchinotogluma segonzaci* had very positive $\delta^{13}C$, suggesting they acquire most of their organic matter from sulfide oxidizers using the reverse tricarboxylic acid (rTCA) cycle[37]. Interestingly, many taxa had intermediate $\delta^{13}C$ values comprised between those two end-members, suggesting a co-reliance on both bacterial metabolisms in variable proportions. Similar findings have been reported for the Manus Basin[32,38]. However, in Manus, communities seem to be mostly supported by the CBB cycle, particularly at the Solwara 1 site[32]. In Woodlark, our results suggest that inter- (and sometimes intra-) taxon differences in feeding preferences could lead to a more evenly balanced continuum of $\delta^{13}C$ values, and therefore the importance of the two production mechanisms for the food web. Finally, $\delta^{34}S$ of Woodlark fauna was similar to some hydrothermal vents from the Manus Basin (Solwara 1, PACMANUS), but markedly higher than other Manus sites (e.g., South Su)[32]. This suggests that local changes in sulfur geochemistry could influence this parameter and the way secondary consumers are locally distributed.

Genetic characterization of the main ecological engineer species

As other vent communities of the western Pacific back-arc basins, engineer species observed at LSVF are mainly composed of stalked barnacles, and provannid gastropods that belong to the genera *Alviniconcha* and *Ifremeria*. *Bathymodiolus* mussel beds

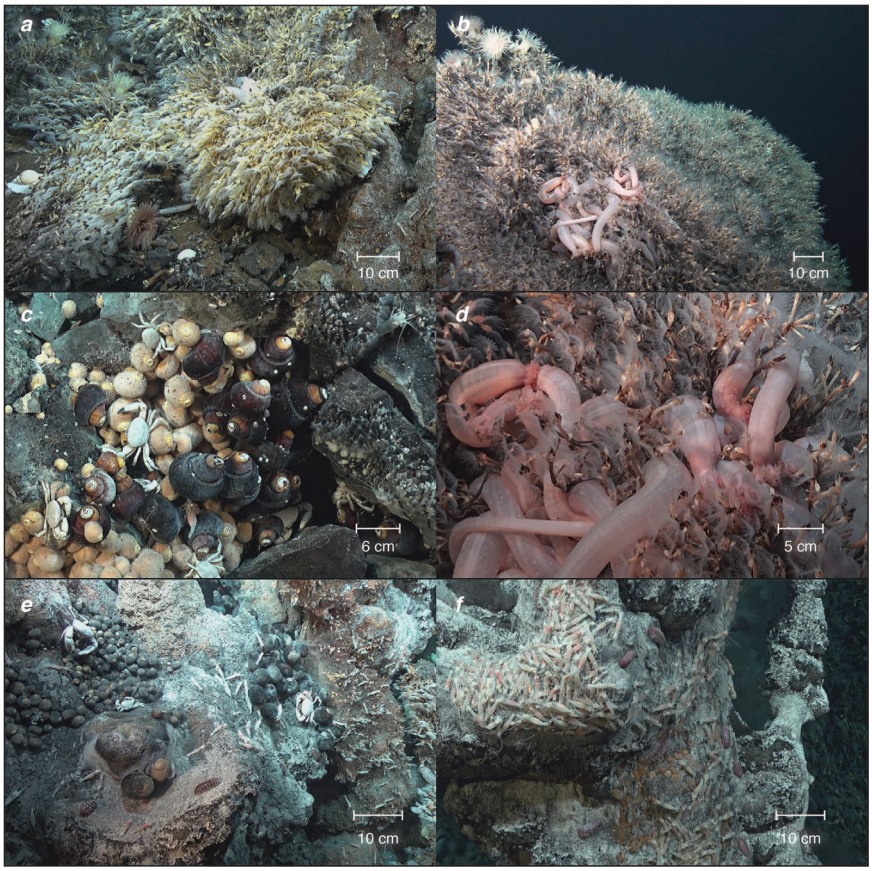

Fig. 5 Hydrothermal fauna from La Scala Vent Field. a *Vulcanolepas* sp. n. thickets, anemones and gastropod *Phymorhynchus* sp. **b** Anemones and holothurian *Chiridota* sp. in *Vulcanolepas* sp. n. thickets. **c** Aggregation of gastropods *Ifremeria nautilei* and *Alviniconcha kojimai* with *Austinograea* crabs and cirripeds *Eochionelasmus ohtai* and *Imbricaverruca* sp. (right side of the picture). **d** *Chiridota* sp. in *Vulcanolepas* sp. n. thicket. **e** Aggregation of *Alviniconcha kojimai*, polynoids, alvinocarids shrimps, and *Austinograea* crabs. **f** Aggregation of alvinocarid shrimp *Rimicaris variabilis*, polynoids *Branchinotogluma segonzaci* and gastropod *Shinkailepas tufari* on active chimney.

were surprisingly not found at Woodlark. A first genetic examination of stalked barnacles using a 658-bp fragment of the mitochondrial cytochrome c oxidase (*Cox1*) gene clearly indicated that, while falling into the *Vulcanolepas* clade (support 0.66), specimens from Woodlark form a distinct phylogenetic clade (support 0.99, within clade pairwise Jukes–Cantor distances $0.22 \pm 0.21\%$) and therefore represent a new putative species (Fig. 7). This new species is surprisingly most closely related to the species found at vents on the Kermadec volcanic arc (*V. osheai*, $6.86 \pm 0.23\%$ average Jukes–Cantor distances), and a bit more distantly to the species found at vents in the Lau Basin (*V. buckeridgei*, $7.35 \pm 0.33\%$ average Jukes–Cantor distances) or the species *Leucolepas longa* from Lihir island[39]. Interestingly, for this genus, each sampled area seems to host a distinct species. *Alviniconcha* and *Ifremeria* gastropods were not numerous (distributed as small patches at the base of chimneys) and of rather small size, suggesting that they may represent genetically differentiated populations when compared to other described species elsewhere. All individuals collected at Woodlark were thus barcoded using a 659 bp-fragment of mitochondrial *Cox1* gene to build haplotype networks and test their relationships with previously described species. For *Alviniconcha*, the use of previously published sequences yielded 5 clusters that correspond to the currently described species. *Alviniconcha* specimens collected at La Scala fall into two equally represented but distinct species, *A. boucheti* and *A. kojimai*, but are not geographically distinct from populations collected in other basins, at least using this genetic marker (Supplementary Fig. 6). *Ifremeria* specimens fall into two main clusters separated by five fixed substitutions (divergence = 0.75%, Fig. 8): one that mainly comprises specimens from the Manus and Woodlark basins and one that comprises specimens from other basins (Lau, North Fiji, and Futuna) (Fig. 8 and Supplementary Fig. 6). Remarkably, a few specimens from Futuna and Lau however, fall into the Manus/Woodlark cluster. This suggests a possible recent migration from the Woodlark ridge to the Northern part of the Lau basin (including Futuna) following a first geographic isolation event of the Manus and Lau/North Fiji/Futuna populations in allopatry. These preliminary results clearly indicate that vent species have contrasted population histories. Some of the species are clearly endemic of the Woodlark ridge (a possible separation due to the greater depth) whereas others may use it as a stepping stone during the colonization of the present-day back-arc basins of the Western Pacific.

The Woodlark Ridge: A potential biological cornerstone?

The tectonic history of the western Pacific back-arc basins is complex[17]. The opening of some basins such as Manus, Lau, and North Fiji is recent (less than 4–3 millions years)[17,40,41], and likely simultaneous, even if the formation of the North Fiji proto-basin initiated before about 10–12 Mya[16]. This points towards the existence of older relay-ridges for the vent fauna before their opening of the present-days basins as previously mentioned to explain the spatial distribution patterns of the symbiotic gastropod *Alviniconcha* spp[18]. In this context, the present-day distribution of the hydrothermal vent fauna likely results from the partition of an older hydrothermal fauna originating from ridges

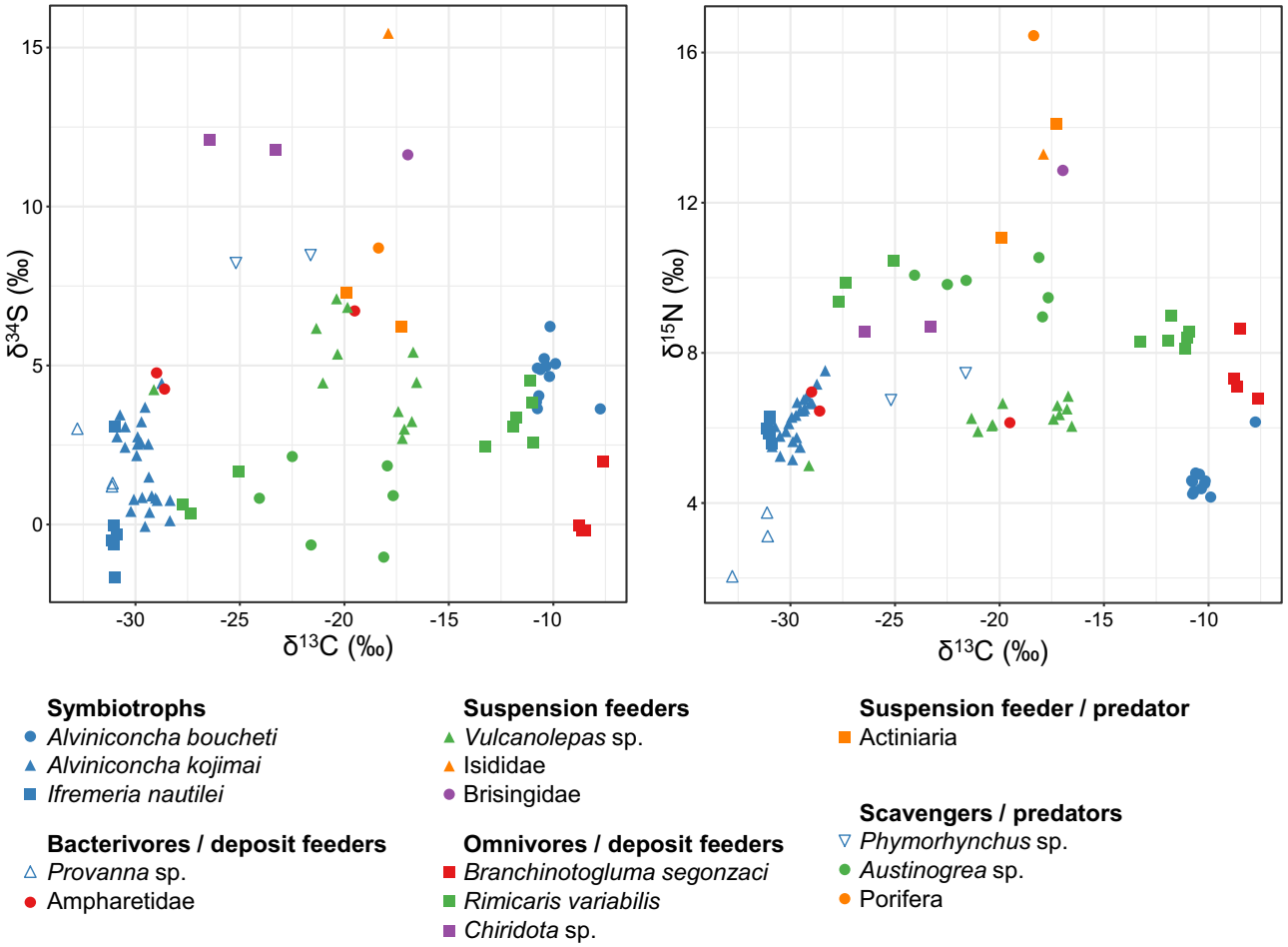

Fig. 6 Stable isotope food web diagram of LSVF animal communities. Stable isotope ratios of carbon vs. sulfur (left) and carbon vs. nitrogen (right) in benthic fauna from La Scala, Woodlark Basin. Blue: molluscs, red: polychaetes, green: crustaceans, orange: sponges and cnidarians, purple: echinoderms. Organisms have been assigned to functional feeding guilds according to literature data.

that have now disappeared by subduction (Fig. 9). The inactive South Fiji or Solomon ridges are relicts of such past ridge systems[17] and may have been transiently linked by the formation of the North Fiji proto-basin after the collision of the Melanesian arc and the Ontong Java plateau about 18 Mya. Amongst back-arc basins, the Woodlark ridge opened (about 6–7 million years[17]) at a time where the northern expansion of the North Fiji proto-basin became extinct, and corresponds to a region that may still contain traces of older dispersal pathways during the Oligocene (i.e., the Solomon Seaway). The Woodlark ridge could thus act as a biodiversity dispersion centre for the modern hydrothermal vent fauna and a crossroad between the Manus, North Fiji, and Lau Basins. To this extent, the discovery of the LSVF on Segment 3 of the Woodlark ridge represents an important opportunity to study the biogeography of the vent fauna associated with back-arc basins. A first examination of our list of species collected at La Scala indicates that the Woodlark assemblage is not noticeably different from other Western Pacific assemblages. It also shows that the basalt-hosted MOR vent system (such as La Scala) and its greater depth do not represent a barrier for most of the vent fauna. Although several studies highlighted genetic differentiation in populations of vent species between the Manus and Lau/Fiji basins[42–44], the addition of populations sampled at Woodlark in genetic analyses will bring further insight into biogeographic patterns and the role of the Woodlark ridge in bridging populations at the regional scale. More population genetics studies using genomic tools are currently underway. So far, the barcoding of symbiotic gastropod species reinforces the view that the Woodlark community, although deep, can be connected to much shallower populations in the Manus Basin (e.g., SuSu volcanoes located nearby, at the opening of the basin) but is also likely to act as a relay for migration between Manus and Fiji/Futuna/Lau, at least for *Ifremeria nautilei* (Fig. 8)[45]. Based on a more general barcoding approach, the Woodlark ridge does not seem to only represent a stepping stone but also a contact zone for some species between these basins (Poitrimol, pers. Comm.). Even if most larval dispersal trajectory modelling in the Southwestern Pacific failed to explain or only weakly explained present-day inter-basin connectivity for the deep-sea fauna even for larvae with a long pelagic duration[46,47], these studies and our own genetic results pointed out the possible role of the Woodlark ridge as a biological cornerstone.

Despite faunal similarities with other Western Pacific communities, communities in the Woodlark Basin may have specific attributes due to the greater depth (3330 mbsl) at which the vent sources are located compared to the shallower vent sites encountered elsewhere in the western Pacific (Manus Pual Ridge, Susu volcanoes, Franklin and Edison seamounts, North Fiji and Lau ridges segments). We found two new species (*Vulcanolepas* sp. nov. and *Austinograea* sp. nov.) at La Scala so far. Further examination of specimens that have been identified at the genus level as the gastropod *Desbruyeresia* or *Provanna* could yield additional new species.

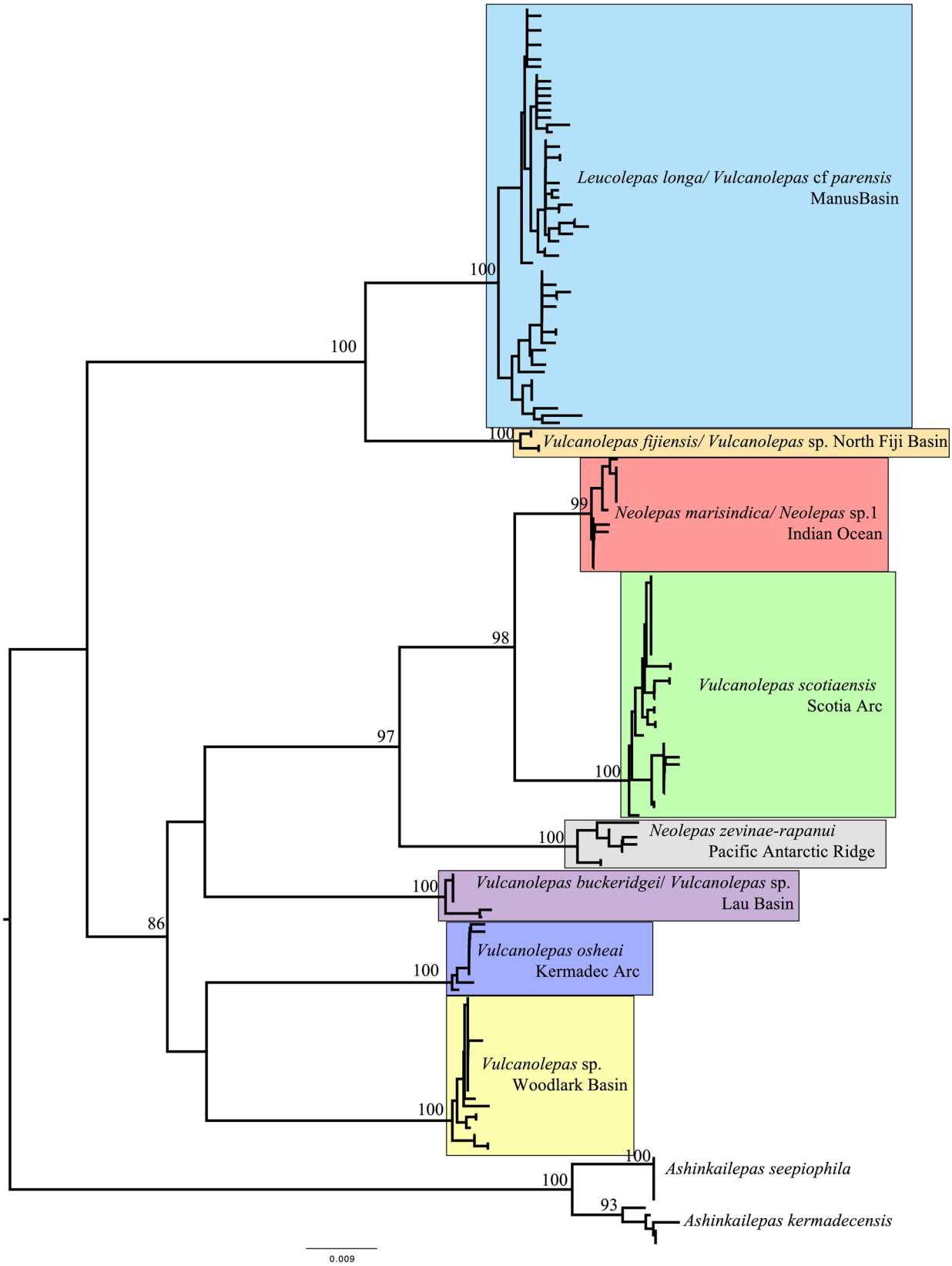

The most striking features of this newly discovered vent assemblage, however, are the scarcity of the symbiotic fauna (no bathymodiolin mussels and small numbers of the large gastropods *Ifremeria nautilei* and *Alviniconcha* spp.) and the astonishing profusion of stalked barnacles (*Vulcanolepas* sp. nov.) that cover most of the vent edifices and their surroundings over nearly 1000 m^2 of basaltic scree. Very extensive dense populations of stalked barnacles have also been observed at Haungaroa (Kermadec Arc, Hourdez, pers. obs.), at deep-sea vents discovered along the flanks of the nearby Edison seamount (near the Lihir island of New Ireland, Papua New Guinea[39]), along the East Scotia Ridge in the Southern Ocean[48] or, along the Southern East

Fig. 7 Phylogenetic network of the LSVF stalked barnacle. Phylogenetic position of the Woodlark stalked barnacle in the genus *Vulcanolepas*. BioNJ tree on Kimura-2-Parameter distances based on a 476 bp alignment of the mitochondrial gene *CoxI*. Numbers above branches are bootstrap values for 100 replicates. Sequences for *Ashinkailepas kermadecensis* and *A. seepiophila* used as outgroup. Accession numbers: *A. kermadecensis* (KP295001, 19, 40, 48, 53, and 61), *A. seepiophila* (KP295022, 28, 31, 46, 69, 90, and 91), *Vulcanolepas* sp. Woodlark (**MW602536-40**, **602552-66**), *Vulcanolepas osheai* (**MW602550-51**, KP295005, 08, 26, 34, 36, 49, 56, and 94), *Vulcanolepas buckeridgei* (KY502196, 97, KP295009, 33, 41, 51, and 80), *Neolepas zevinae rapanui* (KP295007, 55, 60, 63, 67, 84, and 98), *Vulcanolepas scotiaensis* (KP295013, 14, 18, 21, 35, 37, 39, 42, 45, 50, 52, 57, 58, 68, 78, 97, KF739820-38), *Neolepas marisindica/Neolepas* sp. 1 (KP295004, 30, 32, 47, 62, 64, 89, and LC350007-15), *Vulcanolepas fijiensis/Vulcanolepas* sp. (MH636381-83, MN061491), *Leucolepas longa/Vulcanolepas* cf *parensis* (**MW602541-49**, KP295027, 73, 76, 82, 83, 85, and JX036420-64). Accession number that appear in bold were generated for this study.

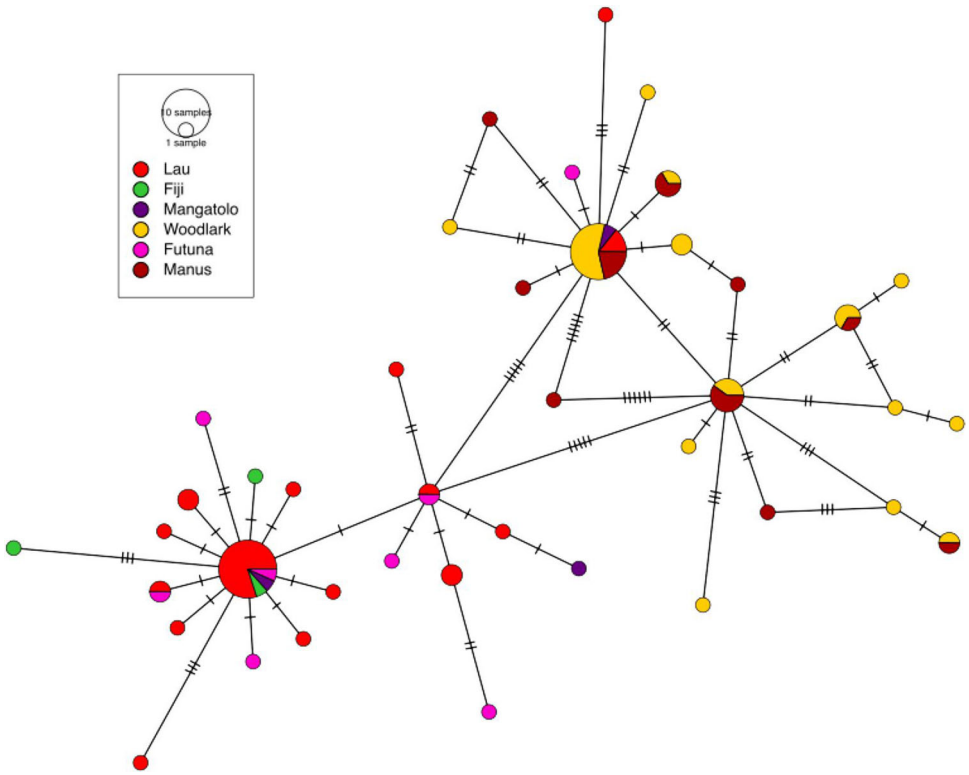

Fig. 8 Haplotype network of the LSVF gastropod *Ifremeria*. Haplotype network of the Woodlark *Ifremeria Cox1* gene (accession numbers: OL448876 - OL448957) with other sequences of geographically referenced individuals using the Median Joining method implemented in the software PopArt[61]. Purple: Woodlark Ridge, pink: Manus basin, Red: Lau basin, Green: North Fiji basin, yellow: Futuna.

Pacific Rise[49]. For each location, however, the stalked barnacle species are clearly different. They probably exploit the suspended particles that can disperse over large distances. This hypothesis is supported by the presence of large bacterial mats at the periphery that most likely also benefit from plume material carried from the main smokers, as observed on the mid-Atlantic ridge[50]. The absence of mussel beds and siboglinid worm agregations, and the fact that symbiotic gastropods are only found in small numbers at the base of the black smoker chimneys do not seem to be attributable to the greater depth of hydrothermal sources. Dense populations of *Alviniconcha* and *Bathymodiolus* have indeed previously been observed at deeper sites (3600 mbsl) on the Mariana Trench[51]. Comparing the vent fauna of Mariana Trench and Mariana Trough (1470 mbsl), Fujikura (1997)[52] concluded that depth had no impact on the species composition of vent communities in the western Pacific. A similar situation was also depicted at the Mid-Caiman Spreading Centre where the community from the Beebe vent field was almost identical to that of the Van Damm vent site, 2000 m shallower[53]. Alternatively, the high number of filter-feeding species (i.e., barnacles) and the reduced, patchy distribution of symbiotic gastropods may represent a transient state of the community where diffuse venting is prevented by focusing the hydrothermal activity into a series of black smokers exporting most of the fluid as high-velocity buoyant plumes that rise to a few tens of metres above the seafloor. This may indicate that the site has recently been reactivated by the tectonic movements that led to the collapse of part of the ridge crest where the emissions have been found, although activity in the general area probably lasted over several thousands of years.

Materials and methods

Bathymetry and acoustic survey. Ship-borne multibeam data were acquired using a Kongsberg EM122 1° × 2° 12 kHz while ROV multibeam data were acquired with a RESON 7125 400 kHz 0.5° × 1°. Both datasets were processed with the GLOBE software (doi.org/10.17882/70460) to provide 20 and 10 m grid (vessel data) and 1 m grid (ROV data) spaced digital terrain models of the surveyed area. The acoustic water column data acquired with the ship-borne 12 kHz MBES at a speed of 8 knots were characterized using the SonarScope (@Ifremer) and GLOBE softwares. Hydrothermal echoes were detected and located by visual inspection of ship-borne water-column polar echograms corresponding to the data of each ping and long-distance echograms associated to the track of the vessel. The most likely position on the seafloor and the maximum height (altitude above the seafloor) of each group of echoes attributed to rising plumes were determined. With this

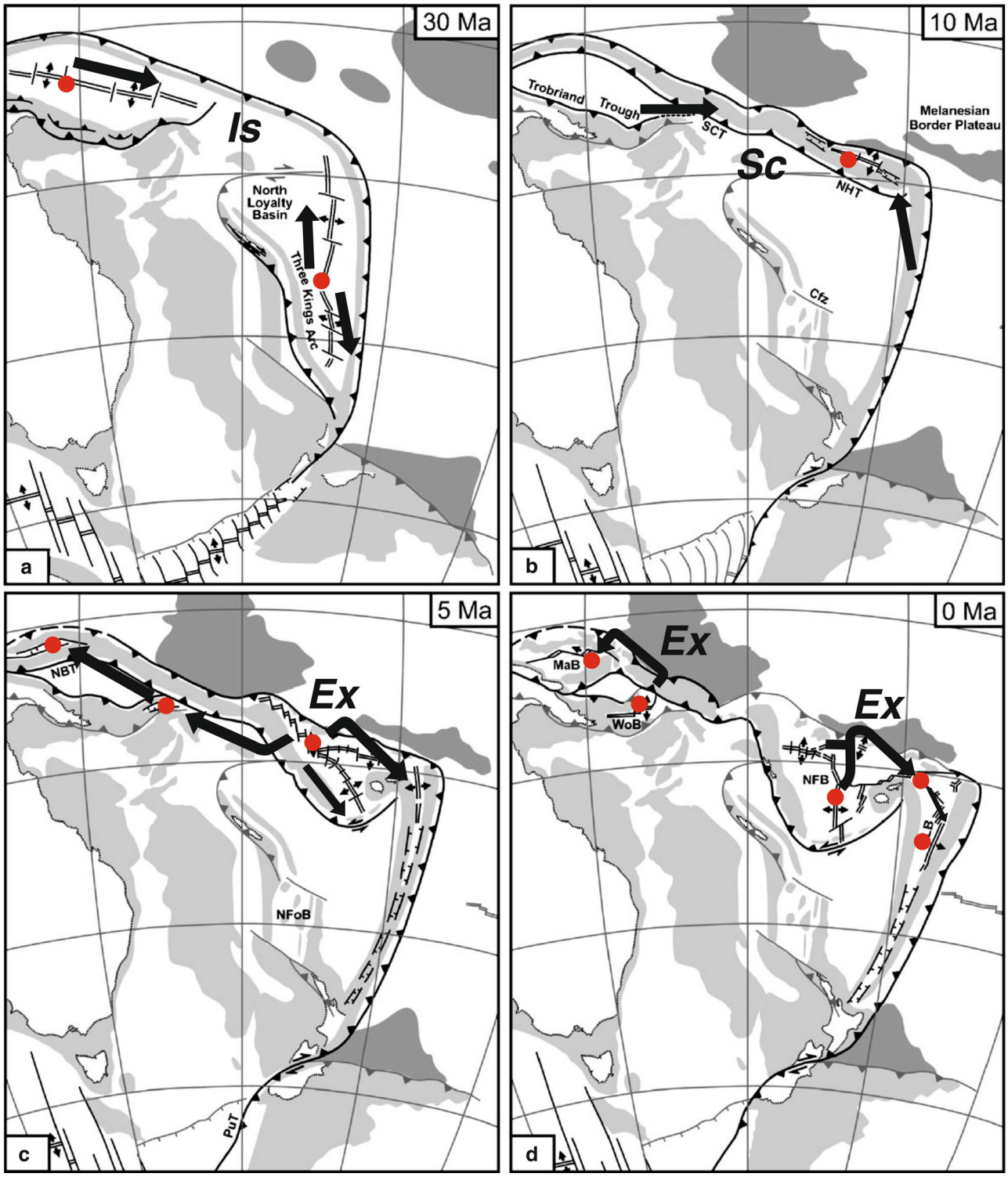

Fig. 9 The Woodlark ridge, a potential biological cornerstone?. Scenario of the Woodlark Ridge's hypothesis as a cornerstone of the vent fauna dispersal in the western Pacific using the geotectonic reconstruction model of the Western back-arc basins adapted from Schellart et al. (2006)[16]. **a** Formation of the Solomon Basin and North Loyalty/South Fiji Basin with two independent ridge systems. **b** Opening of the northern branch of the North Fiji basin after the fossilization of the South Fiji basin and the opening of the Woodlark ridge about 10 Mya. **c** Expansion of North Fiji basin together with the opening of the Lau Basin 5 Mya. **d** Present-days back arc basins with the five hydrothermally active zones, including Futuna. Red dots: active spreading centres, black arrows: putative colonization routes, **Is**: species isolation phase, **Sc**: secondary contact, and **Ex**: population expansion phase.

package, acoustic anomalies were identified, analyzed and attributed to various scatterers (large biological echoes, seafloor reflections…). Anomalies were considered as attributable to hydrothermal plumes if they were connected to the seafloor and reproducible over time, i.e., detected several times at the same location.

Water column operations. All operations were conducted using a 24-Niskin bottle rosette frame onto which were mounted a Seabird CTD 911+, two Turbidimeters (Seapoint Turbidity Metres), a pH sensor (AMT GmBH) and an Eh sensor (AMT GmBH), as well as an altimeter for seafloor detection. The Seasave software provided by Seabird Electronics was used for real-time data acquisition

and display of the down- and up-casts data. Niskin bottles were fired during up-casts at different levels in the water column, whenever an anomaly (T, S, turbidity and Eh) appeared in the real-time data display. The CTD-rosette was deployed in two ways, either as vertical casts or as towed casts ('tow-yos'), which consisted in lowering and raising the CTD-rosette between a constant set depth and ~100 m above the seafloor while the ship moved along a transect at a maximum speed of 1 knot. Vertical casts were stopped 5 m above the seafloor (provided by the altimeter).

Water samples were drawn from the Niskin bottles, fitted with Teflon stopcocks and sealed with Viton O-rings, both compatible with metal analyses. All subsamples were fully processed within 4 h after the CTD-rosette arrived on deck. Several types of samples were collected: (1) unfiltered water used for total dissolvable metal concentrations after acidification to pH 1.8; (2) water filtered directly from the niskin bottles using gravity flow through acid-cleaned Acropak® filters equipped with 0.45 um Supor® Membrane. All fluid transfers from the Niskin bottles were performed under controlled conditions designed to avoid shipborne contaminations, including the use of acid-clean tubing and sampling LDPE bottles placed inside double plastic bags and protected by filling bell outlet. Each precleaned LDPE bottle was rinsed 3 times with seawater sample before final filling. All samples were acidified to pH 1.8 with Optima-grade HCl inside a clean-air flow bench and analyzed back onshore for dissolved and total dissolvable metals (including Mn).

Hydrothermal fluid sampling. The hydrothermal fluid from each black smoker chimney was sampled in duplicate into two 750 mL syringe-style Titanium samplers manipulated by the ROV arm to estimate concentrations of end-members. In total, six samples of fluids from three chimneys were recovered immediately after removing the top of the chimney and measuring temperature with the ROV probe. Temperature was also recorded in real-time during the fluid collection using thermocouple temperature probes (NKE® probes) mounted on the sampler snorkel. Fluids were processed on board straight away after recovery using the following scheme:

i. Aliquots were also transferred directly into evacuated glass bottles that contain a pre-weighed amount of Zn-acetate [$Zn(CH_3COO)_2$~$2H_2O$] to precipitate ZnS for $\delta^{34}S$ and H_2S concentration (i.e., total HS^-) measurements.
ii. Aliquots were then collected for shipboard analysis (pH and total HS^- using either titration or Cline, method[54] depending on the concentration).
iii. The remaining fluid solutions in the Ti-samples were then transferred into an acid cleaned 1 L HDPE bottle and homogenized before further separated into aliquots for on shore analyses: ion chromatrographic analysis (major cations/anions; data not reported here); HR-ICPMS (major and trace elements); silica concentration after 100-fold dilution with ultra-pure water to prevent silica precipitation. Due to the high concentrations of metals in the hydrothermal solutions, precipitation often occurs within the titanium samplers as they cool down to ambient temperature. Those particles were found to be nearly entirely transferred into the 1 L HDPE bottle. Precipitated particles remaining in the Ti-samplers were however recovered for chemical analysis when the samplers are disassembled by rinsing with Milli-Q water and ethanol, and filtered through 0.45 µm filters. This fraction is hereafter referred to as "dregs" (not reported here).

On shore fluid analyses. Major and trace elements were measured by high-resolution inductively coupled plasma mass spectrometry (HR-ICPMS) Element XR operated at the French Research Institute for Exploitation of the Sea (IFREMER). Indium solution was added before analysis or mixed on-line at a final concentration of 5 ppb to correct for instrument sensitivity changes. Solutions were diluted 100-fold and introduced into the plasma torch using a quartz spray chamber system equipped with a microconcentric PFA nebulizer operating at a flow rate of about 60 µl/min. For each element, ICPMS sensitivity was calibrated using matrix matched standard solutions corresponding to seawater matrices. Anions (Cl, SO_4) were analyzed by ionic chromatography after appropriate dilutions.

Sulfide analysis (XRF, XRD, HR-ICPMS, $\delta^{34}S$). Rock and sulfide samples collected during the dives were petrographically characterized directly on-board. Two types of subsamples were considered: A representative portion of the sample (referred as bulk) or mineral separates. Both sample types were dried in an air oven at 50 °C and ground to a fine powder using an agate mortar.

Mineralogical and quantitative chemical data were acquired using X-ray techniques (XRD and X-ray fluorescence) at the Laboratoire de Géochimie et Métallogénie at IFREMER. XRD analyses were conducted with a BRUKER AXS D8 Advance diffractometer. Samples were top loaded into 2.5 cm-diameter circular cavity holders, and analyses were run between 5° and 70° 2θ, in steps of 0.01° 2θ at 1 s/step (monochromatic Cu Kα radiation, 40 kV, 30 mA). Minerals were identified using the Diffrac suite EVA software.

X-ray fluorescence analyses were conducted with a wavelength dispersive X-ray fluorescence spectrometer (WD-XRF; BRUKER AXS S8 TIGER) on fusion beads (for major elements) or compressed pellets (for trace elements). After data acquisition, the measured net peak intensities, corrected for inter-element effects, were converted into concentrations using calibration curves generated from analysis of certified geochemical standard powders (measured under identical analytical conditions). Calibrations were established using a set of certified materials obtained mainly from the Canadian Certified reference materials Project (CCRMP) (for example, CCU-1, CZN-1, Fer-1, PTC-1 or PTM-1), Geological Survey of Japan (GSJ)(JP-1), and the Centre de Recherches Pétrochimiques et Géochimiques in France (CRPG)(BE-N).

For sulfur isotopes, sample powder was digested in inverted aqua regia and then purified by elution through a cationic resin to remove any interfering matrix. The solution was analyzed by a Neptune MC-ICP-MS at Ifremer following the procedure of Craddock et al. (2008)[55] and calibrated against a set of internal and external standards (IAEA NZ-1, NZ-2, NZ-4, NBS 123).

All mineral samples were also analyzed for major and trace elements by HR-ICPMS at IFREMER. About 100 mg of dry powder was dissolved in a PTFE beaker on a hot plate using an acid mixture of HCl, and HNO_3. Digested samples were then further diluted 50-fold and analyzed by HR-ICPMs following similar approaches than for fluid samples described above. A set of international georeference materials (e.g., BHVO-2, GH, UB-N, NOD-P-1, IF-G, NIST2711) and internal standard solutions relevant to sulfide-rich samples were used to calibrate the measurements.

Sampling and preservation of animals. Benthic macrofauna was collected using the claw of the hydraulic arm of the ROV Victor 6000 and placed into collection boxes. The remaining fauna on the substrate was then sampled with the suction sampler of the ROV equipped with a 1 mm mesh. Three benthic communities defined by engineer species were specifically sampled over an area of about 0.5 m^2 (i.e., one sample for the *Vulcanolepas* community, one sample for the *Ifremeria* community and two samples for the *Alviniconcha* community). Temperature measurements were made at three locations using the ROV temperature probe prior and after sampling for *Ifremeria* and *Alviniconcha* communities. In addition, opportunistic sampling was carried out to collect organisms found on the black smokers (e.g., polynoid worms, crabs and shrimp) and peripheral area using the robotic arm and claw of the ROV. This sampling was supplemented by observations performed with the high-definition video camera of the ROV for large megafauna. Onboard, samples were sieved on a 250 µm sieve, and all organisms were sorted and preserved in 96° ethanol before their identification at the lowest taxonomic level based on morphological criteria. Some specimens of each species were also frozen at −80 °C in order to perform stable isotopes (^{13}C, ^{15}N, and ^{34}S) analyses.

Stable isotope analyses. On board, animals were dissected to separate soft and non-metabolically active tissues (e.g., muscle, tegument) or, when body size was small, were used whole[56]. All samples were oven-dried at 60 °C for 72 h, then placed in airtight containers and kept at room temperature before further treatment once back from the expedition. They were subsequently ground to a homogeneous powder using mortar and pestle. Samples containing hard inorganic carbon parts that could not be physically removed were acidified by exposing them to HCl vapours for 48 h in an airtight container[57]. Stable isotope ratios measurements were performed via continuous flow—elemental analysis— isotope ratio mass spectrometry (CF-EA-IRMS) at University of Liège (Belgium), using a vario MICRO cube C–N–S elemental analyzer (Elementar Analysensysteme GMBH, Hanau, Germany) coupled to an IsoPrime100 isotope ratio mass spectrometer (Isoprime, Cheadle, United Kingdom). Isotopic ratios were expressed using the widespread δ notation[58], in ‰ and relative to the international references Vienna Pee Dee Belemnite (for carbon), Atmospheric Air (for nitrogen) and Vienna Canyon Diablo Troilite (for sulfur). IAEA (International Atomic Energy Agency, Vienna, Austria) certified reference materials sucrose (IAEA-C-6; $\delta^{13}C = -10.8 \pm 0.5$‰; mean ± SD), ammonium sulfate (IAEA-N-2; $\delta^{15}N = 20.3 \pm 0.2$‰; mean ± SD) and silver sulfide (IAEA-S-1; $\delta^{34}S = -0.3$‰) were used as primary analytical standards. Sulfanilic acid (Sigma-Aldrich; $\delta^{13}C = -25.6 \pm 0.4$‰; $\delta^{15}N = -0.13 \pm 0.4$‰; $\delta^{34}S = 5.9 \pm 0.5$‰; means ± SD) was used as secondary analytical standard. Standard deviations on multi-batch replicate measurements of secondary and internal lab standards (amphipod crustacean muscle) analyzed interspersed with samples (one replicate of each standard every 15 analyses) were 0.2‰ for both $\delta^{13}C$ and $\delta^{15}N$ and 0.5‰ for $\delta^{34}S$.

Genetic analyses

Barcoding analyses. Genomic DNA from gastropod, barnacle and crab specimens collected from the site La Scala were extracted using a CTAB extraction procedure. Tissues were digested overnight in 600 µl of a 1% CTAB buffer solution (1.4-M NaCl, 0.2% 2-mercaptoethanol, 20 mM EDTA, 100-mM Tris-HCl pH 8 and 0.1 mg ml^{-1} proteinase K) also containing 1% PVPP (PolyVinylPolypyrolidone). DNA was then extracted by adding chloroform–isoamyl alcohol (24:1), precipitated with 1 ml of cold 100% ethanol, washed with 70% ethanol and resuspended in 100 µl of sterile solution of 0.1X TE (Tris EDTA pH 8.0). For shrimp, genomic DNA was extracted using E.Z.N.A. Tissue DNA kit (Omega Bio-Tek) according to the manufacturer's recommendations. For the mt *Cox1* gene,

amplifications were performed in 25 µl final volume using the 'universal' applicable primers of Folmer et al. (1994)[59] and the following conditions: 1× reaction buffer), 2.5 mM $MgCl_2$, 0.12 mM of each dNTP, 0.38 µM of each primers, 1U Taq DNA polymerase (Uptitherm), 2.5 µl of template DNA and sterile H_2O. Thermal cycling parameters used an initial denaturation at 94 °C for 2 min, followed by 35 cycles at 94 °C for 30 s, 50 °C for 1 min, 72 °C for 2 min and a final 5 min extension cycle. An alternative protocol was used for shrimp with specific primers for alvinocaridid shrimp[60].

Phylogenetic and haplotype networks. A phylogenetic tree was produced determine the position of the new pedunculate cirriped by a PhyML approach using a general time reversible model of substitutions with a Gamma distribution of the substitution rate. This latter rate, nucleotide equilibrium frequencies, and the proportion of invariant sites were optimized by the search algorithm. Node confidence was evaluated with an αLRT (SH-like) approach. Haplotype networks for the gastropods were produced using the minimum spanning method implemented in PopArt[61] on mt*Cox1* alignments of the three main symbiotic gastropod species.

Reporting summary. Further information on research design is available in the Nature Research Reporting Summary linked to this article.

Data availability

The datasets generated during the current study are available at https://doi.org/10.6084/m9.figshare.19095659. All bathymetric data and sampling metadata from the cruise are available at https://doi.org/10.17600/18001111.

Received: 27 April 2021; Accepted: 11 February 2022;
Published online: 17 March 2022

References

1. German, C. R. & Von Damm, K. L. *Treatise on Geochemistry* (eds Heinrich, D. H. & Karl, K. T.) 181–222 (Pergamon, 2003).
2. Van Dover, C. *The Ecology of Deep-Sea Hydrothermal Vents* (Princeton University Press, 2000).
3. Spiess, F. N. et al. East Pacific rise: Hot springs and geophysical experiments. *Science* **207**, 1421–1433 (1980).
4. Haymon, R. M. et al. Hydrothermal vent distribution along the East Pacific Rise crest 9° 09'–54' N and its relationship to magmatic and tectonic processes on fast-spreading mid-ocean ridges. *Earth Planetary Sci. Lett.* **104**, 513–534 (1991).
5. Edmonds, H. N. et al. Discovery of abundant hydrothermal venting on the ultraslow-spreading Gakkel Ridge in the Arctic Ocean. *Nature* **421**, 252–256 (2003).
6. German, C. R. et al. Hydrothermal activity and seismicity at Teahitia Seamount: Reactivation of the society islands hotspot? *Front. Mar. Sci* **7**, 73 (2020).
7. de Ronde, C. E. J. et al. Intra-oceanic subduction-related hydrothermal venting, Kermadec volcanic arc, New Zealand. *Earth Planetary Sci. Lett.* **193**, 359–369 (2001).
8. Ishibashi, J. & Urabe, T. *Backarc Basins: Tectonics and Magmatism* (ed Taylor, B.) 451–495 (Springer, 1995).
9. Fouquet, Y. et al. Hydrothermal activity and metallogenesis in the Lau back-arc basin. *Nature* **349**, 778–781 (1991).
10. Boschen, R. E., Rowden, A. A., Clark, M. R. & Gardner, J. P. A. Mining of deep-sea seafloor massive sulfides: A review of the deposits, their benthic communities, impacts from mining, regulatory frameworks, and management strategies. *Ocean Coastal Manage.* **84**, 54–67 (2013).
11. Lisitsyn, A. P. et al. Active hydrothermal activity at Franklin Seamount, Western Woodlark Sea (Papua New Guinea). *Int. Geol. Rev.* **33**, 914–929 (1991).
12. Laurila, T. E. et al. Tectonic and magmatic controls on hydrothermal activity in the Woodlark Basin: Hydrothermalism in the Woodlark Basin. *Geochem. Geophys. Geosyst.* **13**, Q09006 (2012).
13. Goodliffe, A. M. et al. Synchronous reorientation of the Woodlark Basin spreading center. *Earth Planetary Sci. Lett.* **146**, 233–242 (1997).
14. Martínez, F., Taylor, B. & Goodliffe, A. M. Contrasting styles of seafloor spreading in the Woodlark Basin: Indications of rift-induced secondary mantle convection. *J. Geophys. Res.* **104**, 12909–12926 (1999).
15. Taylor, B., Goodliffe, A., Martinez, F. & Hey, R. Continental rifting and initial sea-floor spreading in the Woodlark Basin. *Nature* **374**, 534–537 (1995).
16. Schellart, W. P., Lister, G. S. & Toy, V. G. A Late Cretaceous and Cenozoic reconstruction of the Southwest Pacific region: Tectonics controlled by subduction and slab rollback processes. *Earth-Sci. Rev.* **76**, 191–233 (2006).
17. Hall, R. Cenozoic geological and plate tectonic evolution of SE Asia and the SW Pacific: Computer-based reconstructions, model and animations. *J. Asian Earth Sci.* **20**, 353–431 (2002).
18. Breusing, C. et al. Allopatric and sympatric drivers of speciation in Alviniconcha hydrothermal vent snails. *Mol. Biol. Evol.* **37**, 3469–3484 (2020).
19. Ondréas, H., Scalabrin, C., Fouquet, Y. & Godfroy, A. Recent high-resolution mapping of Guaymas hydrothermal fields (Southern Trough). *BSGF - Earth Sci. Bull.* **189**, 6 (2018).
20. Nakamura, K. et al. Water column imaging with multibeam echo-sounding in the mid-Okinawa Trough: Implications for distribution of deep-sea hydrothermal vent sites and the cause of acoustic water column anomaly. *Geochem. J.* **49**, 579–596 (2015).
21. Xu, G., Jackson, D. R. & Bemis, K. G. The relative effect of particles and turbulence on acoustic scattering from deep sea hydrothermal vent plumes revisited. *J. Acoust. Soc. Am.* **141**, 1446–1458 (2017).
22. Park, S.-H. et al. Petrogenesis of basalts along the eastern Woodlark spreading center, equatorial western Pacific. *Lithos* **316–317**, 122–136 (2018).
23. Chadwick, J. et al. Arc lavas on both sides of a trench: Slab window effects at the Solomon Islands triple junction, SW Pacific. *Earth Planetary Sci. Lett.* **279**, 293–302 (2009).
24. Fouquet, Y. et al. *Geodiversity of Hydrothermal Processes Along the Mid-Atlantic Ridge and Ultramafic-Hosted Mineralization: A New Type of Oceanic Cu-Zn-Co-Au Volcanogenic Massive Sulfide Deposit* (eds Rona, P. A., Devey, C. W., Dyment, J. & Murton, B. J.) Vol. 188, 321–367 (American Geophysical Union, 2010).
25. Von Damm, K. et al. Chemistry of submarine hydrothermal solutions at 21N, East Pacific Rise. *Geochim. Cosmochim. Acta* **49**, 2197–2220 (1985).
26. Seyfried, W. E. & Bischoff, J. L. Experimental seawater-basalt interaction at 300 °C, 500 bars, chemical exchange, secondary mineral formation and implications for the transport of heavy metals. *Geochim. Cosmochim. Acta* **45**, 135–147 (1981).
27. Pester, N. J., Rough, M., Ding, K. & Seyfried, W. E. A new Fe/Mn geothermometer for hydrothermal systems: Implications for high-salinity fluids at 13°N on the East Pacific Rise. *Geochim. Cosmochim. Acta* https://doi.org/10.1016/j.gca.2011.08.043 (2011).
28. Podowski, E. L., Moore, T. S., Zelnio, K. A., Luther, G. W. & Fisher, C. R. Distribution of diffuse flow megafauna in two sites on the Eastern Lau Spreading Center, Tonga. *Deep Sea Res. Part I: Oceanogr. Res. Papers* **56**, 2041–2056 (2009).
29. Collins, P., Kennedy, R. & Van Dover, C. A biological survey method applied to seafloor massive sulphides (SMS) with contagiously distributed hydrothermal-vent fauna. *Mar. Ecol. Prog. Ser.* **452**, 89–107 (2012).
30. Desbruyères, D., Hashimoto, J. & Fabri, M.-C. Composition and biogeography of hydrothermal vent communities in Western Pacific back-arc basins. *Geophys. Monogr. Ser.* **166**, 215–234 (2006).
31. Reid, W. D. K. et al. Spatial differences in East scotia ridge hydrothermal vent food webs: Influences of chemistry, microbiology, and predation on trophodynamics. *PLoS One* **8**, e65553 (2013).
32. Van Audenhaege, L., Fariñas-Bermejo, A., Schultz, T. & Lee Van Dover, C. An environmental baseline for food webs at deep-sea hydrothermal vents in Manus Basin (Papua New Guinea). *Deep Sea Res. Part I: Oceanogr. Res. Papers* https://doi.org/10.1016/j.dsr.2019.04.018 (2019).
33. Erickson, K. L., Macko, S. A. & Van Dover, C. L. Evidence for a chemoautotrophically based food web at inactive hydrothermal vents (Manus Basin). *Deep-Sea Res. Part II: Top. Stud. Oceanogr.* **56**, 1577–1585 (2009).
34. Comeault, A., Stevens, C. J. & Juniper, S. K. Mixed photosynthetic-chemosynthetic diets in vent obligate macroinvertebrates at shallow hydrothermal vents on Volcano 1, South Tonga Arc—evidence from stable isotope and fatty acid analyses. *Cahiers de Biologie Marine* **51**, 351–359 (2010).
35. Bennett, S. A., Dover, C. V., Breier, J. A. & Coleman, M. Effect of depth and vent fluid composition on the carbon sources at two neighboring deep-sea hydrothermal vent fields (Mid-Cayman Rise). *Deep-Sea Res. Part I: Oceanogr. Res. Papers* **104**, 122–133 (2015).
36. Levin, L. A. et al. Hydrothermal vents and methane seeps: Rethinking the sphere of influence. *Front. Marine Sci.* **3**, 1–23 (2016).
37. Hügler, M. & Sievert, S. M. Beyond the Calvin cycle: Autotrophic carbon fixation in the ocean. *Annu. Rev. Mar. Sci.* **3**, 261–289 (2011).
38. Wang, X., Li, C., Wang, M. & Zheng, P. Stable isotope signatures and nutritional sources of some dominant species from the PACManus hydrothermal area and the Desmos caldera. *PLoS One* **13**, e0208887 (2018).
39. Tunnicliffe, V. & Southward, A. J. Growth and breeding of a primitive stalked barnacle Leucolepas longa (Cirripedia: Scalpellomorpha: Eolepadidae: Neolepadinae) inhabiting a volcanic seamount off Papua New Guinea. *J. Mar. Biol. Ass.* **84**, 121–132 (2004).
40. Auzende, J. M., Pelletier, B. & Lafoy, Y. Twin active spreading ridges in the North Fiji Basin (southwest Pacific). *Geology* **22**, 63–66 (1994).
41. Parson, L. M. & Wright, I. C. The Lau-Havre-Taupo back-arc basin: A southward-propagating, multi-stage evolution from rifting to spreading. *Tectonophysics* **263**, 1–22 (1996).

42. Thaler, A. D. et al. Comparative population structure of two deep-sea hydrothermal-vent-associated decapods (Chorocaris sp. 2 and Munidopsis lauensis) from Southwestern Pacific back-arc basins. *PLoS One* **9**, e101345 (2014).
43. Lee, W.-K., Kim, S.-J., Hou, B. K., Van Dover, C. L. & Ju, S.-J. Population genetic differentiation of the hydrothermal vent crab Austinograea alayseae (Crustacea: Bythograeidae) in the Southwest Pacific Ocean. *PLoS One* **14**, e0215829 (2019).
44. Plouviez, S. et al. Amplicon sequencing of 42 nuclear loci supports directional gene flow between South Pacific populations of a hydrothermal vent limpet. *Ecol. Evol.* https://doi.org/10.1002/ece3.5235 (2019).
45. Tran Lu Y, A. et al. Fine-scale genomic patterns of connectivity in the deep sea hydrothermal gastropod Ifremeria nautilei over its species range using outlier scans and demo-genetic inferences. *Mol. Ecol.* (In Revision).
46. Yearsley, J. M. & Sigwart, J. D. Larval transport modeling of deep-sea invertebrates can aid the search for undiscovered populations. *PLoS One* **6**, e23063 (2011).
47. Mitarai, S., Watanabe, H., Nakajima, Y., Shchepetkin, A. F. & McWilliams, J. C. Quantifying dispersal from hydrothermal vent fields in the western Pacific Ocean. *Proc. Natl Acad. Sci. USA* **113**, 2976–2981 (2016).
48. Marsh, L. et al. Microdistribution of faunal assemblages at deep-sea hydrothermal vents in the southern ocean. *PLoS One* **7**, e48348 (2012).
49. Jollivet, D. et al. The Biospeedo cruise: A new survey of hydrothermal vents along the south East Pacific Rise from 7°24' S to 21°33' S. *InterRidge News* **13**, 20–26 (2005).
50. Girard, F. et al. Currents and topography drive assemblage distribution on an active hydrothermal edifice. *Prog. Oceanogr.* **187**, 102397 (2020).
51. Hessler, R. R. & Lonsdale, P. F. Biogeography of Mariana Trough hydrothermal vent communities. *Deep Sea Res. Part A. Oceanogr. Res. Papers* **38**, 185–199 (1991).
52. Fujikura, K. Biology and earth scientific investigation by the submersible 'Shinkai 6500' system of deep-sea hydrothermal and lithosphere in the Mariana back-arc basin. *JAMSTEC J. Deep Sea Res.* **13**, 1–20 (1997).
53. Connelly, D. P. et al. Hydrothermal vent fields and chemosynthetic biota on the world's deepest seafloor spreading centre. *Nat. Commun.* **3**, 620 (2012).
54. Cline, J. D. Spectrophotometric determination of hydrogen sulfide in natural waters. *Limnol. Oceanogr.* **14**, 454–458 (1969).
55. Craddock, P. R., Rouxel, O. J., Ball, L. A. & Bach, W. Sulfur isotope measurement of sulfate and sulfide by high-resolution MC-ICP-MS. *Chem. Geol.* **253**, 102–113 (2008).
56. Mateo, M. A., Serrano, O., Serrano, L. & Michener, R. H. Effects of sample preparation on stable isotope ratios of carbon and nitrogen in marine invertebrates: Implications for food web studies using stable isotopes. *Oecologia* **157**, 105–115 (2008).
57. Hedges, J. I. & Stern, J. H. Carbon and nitrogen determinations of carbonate-containing solids1. *Limnol. Oceanogr.* **29**, 657–663 (1984).
58. Coplen, T. B. Guidelines and recommended terms for expression of stable-isotope-ratio and gas-ratio measurement results: Guidelines and recommended terms for expressing stable isotope results. *Rapid Commun. Mass Spectrom.* **25**, 2538–2560 (2011).
59. Folmer, O., Black, M., Hoeh, W., Lutz, R. & Vrijenhoek, R. DNA primers for amplification of mitochondrial cytochrome c oxidase subunit I from diverse metazoan invertebrates. *Mol. Mar. Biol. Biotechnol.* **3**, 294–299 (1994).
60. Methou, P., Michel, L. N., Segonzac, M., Cambon-Bonavita, M.-A. & Pradillon, F. Integrative taxonomy revisits the ontogeny and trophic niches of *Rimicaris* vent shrimps. *R. Soc. Open Sci.* **7**, 200837 (2020).
61. Leigh, J. W. & Bryant, D. Popart: Full-feature software for haplotype network construction. *Methods Ecol. Evol.* **6**, 1110–1116 (2015).

Acknowledgements

We are deeply grateful to the captain and crew of the French Research Vessel L'Atalante and to the team in charge of the ROV 6000 Victor without whom nothing would have been possible. We also thank Delphine Pierre (Ifremer CTDI) and Emilie Hardouin (Genavir) for their assistance in the production of the High-Resolution Bathymetric Chart of the Woodlark Ridge, as well as Anne-Sophie Alix (Ifremer GM) with the Geographic Information System. We finally thank Claire Daguin-Thiébaut, Stéphanie Ruault and Marion Ballenghien (Station Biologique de Roscoff) for their assistance in the molecular analyses. This work benefited from access to the Biogenouest genomic platform at Station Biologique de Roscoff. The authors would also like to dedicate this article to Jean-Marie Auzende who spent a large part of his life exploring the oceanic ridges of the Western Pacific to better understand the plate dynamics in this region. Finally, we thank the three anonymous reviewers for the useful comments in improving the manuscript. Ship time was supported by the French Oceanographic Fleet while scientific work was funded through the ANR 'CERBERUS' (contract number ANR-17-CE02-0003).

Author contributions

The cruise was led by D.J. and S.H. as co-principal investigators. They also acquired the genetic data on specimens collected during the cruise. C.B. is the coordinator of the present article and was responsible for the water column survey; O.R. was responsible for the geochemical analysis of the rocks and mineralization as well as the geochemical composition of the water column; C.S. was responsible for the acquisition of bathymetry and the processing of the acoustic data (ship and ROV); P.L.M. participated in the pre-treatment of the bathymetry data on board and produced the high-resolution bathymetric map; E.P. (not onboard) helped in the interpretation of the geological structures and geochemical composition of the fluids observed during the surveys; C.C. (not onboard) was responsible for the fluid sampling equipment and helped in the data processing from the CTD; C.P., E.T., and M.M. (not onboard) were responsible for the description of the fauna and the ecology of the sites; J.C. (not onboard) and A.T.L.Y. participated in the genetic analyses of the targeted fauna collected at LSVF. S.C. (not onboard) and A.B. (not onboard) produced the X-ray data; Y.G. carried out the analyses for the isotopic composition of fluids and mineralization; V.G. was in charge of hydrothermal fluids analysis (IC); L.M. investigated the isotopic ratios across the food web; S.A.-H., F.B., T.B., V.C.-.G., V.L.L., S.L'.H., J.M., A.-S.L.P., A.T., and D.C. Kuama participated and contributed to the sampling and data acquisition during the CHU-BACARC Cruise (doi: 10.17600/18001111) during which the La Scala Vent field was discovered.

Competing interests

The authors declare no competing interests.

Additional information

Supplementary information The online version contains supplementary material available at https://doi.org/10.1038/s43247-022-00387-9.

Correspondence and requests for materials should be addressed to Cédric Boulart.

Peer review information *Communications Earth & Environment* thanks the anonymous reviewers for their contribution to the peer review of this work. Primary Handling Editors: Maria-Luce Frezzotti and Clare Davis.

Reprints and permission information is available at http://www.nature.com/reprints

Publisher's note Springer Nature remains neutral with regard to jurisdictional claims in published maps and institutional affiliations.

Open Access This article is licensed under a Creative Commons Attribution 4.0 International License, which permits use, sharing, adaptation, distribution and reproduction in any medium or format, as long as you give appropriate credit to the original author(s) and the source, provide a link to the Creative Commons license, and indicate if changes were made. The images or other third party material in this article are included in the article's Creative Commons license, unless indicated otherwise in a credit line to the material. If material is not included in the article's Creative Commons license and your intended use is not permitted by statutory regulation or exceeds the permitted use, you will need to obtain permission directly from the copyright holder. To view a copy of this license, visit http://creativecommons.org/licenses/by/4.0/.

© The Author(s) 2022